Proceedings of the 17th World Congress
The International Federation of Automatic Control
Seoul, Korea, July 6-11, 2008

SLAM Using Single Laser Range Finder

AliAkbar Aghamohammadi, Amir H. Tamjidi, Hamid D. Taghirad
Advance Robotic and Automation Systems Lab (ARAS),
Electrical and Computer Engineering Department
K. N. Toosi University of Technology, Iran

Abstract: Presented method in this paper aims to develop an accurate motion model and SLAM algorithm, which is only based on the Laser Range Finder (LRF) data. Proposed method tries to overcome some practical problems in traditional motion models and SLAM approaches, such as robot slippage, and inaccuracy in parameters related to robot's hardware. Novel insights specific to process and measurement model, and making use of them in the IEKF framework, give rise to the real time method with drift-free performance in restricted environments. Furthermore, uncertainty measures, calculated through the method, are valuable information for fusion purposes and also an accurate motion model, derived in this method, can be used as a robust and an accurate localization procedure in different structured environments. These issues are validated through experimental implementations; experiments verify method's efficiency both in pure localization and in SLAM scenarios in the restricted environments, involving loop closures.

1. INTRODUCTION

Simultaneous Localization and Mapping (SLAM) has received immense attention of many researchers in the last 20 years. SLAM has been formulated in different frameworks; however, crossing over into practical systems confronts with substantial issues. Focus of the work presented here is on developing a theory, which can overcome some problems, come into view in practical implementations. The problems, considered here, stem from unmodeled dynamics of the system, such as robot slippage, surface type changing, and imprecision in the parameters of robot's hardware. In other words, method aims to circumvent traditional encoder-base dynamic modeling and propose a robust process model with respect to mentioned problems.

The key contributions given in this paper include accurate covariance calculation for robot displacement derived from feature based laser scan matching, and the use of this information to establish a robust motion model. This is accomplished based on extracted features' individual covariances. Exploiting calculated covariance and features' individual covariances, the Extended Kalman Filter (EKF) framework, is established to estimate robot's and features' states, only based on the laser range finder information. Together, these add up to an efficient and robust algorithm achieves real time implementation with single LRF hardware.

To fuse the LRF data with the other sensors, it is necessary to calculate reliability of obtained information. This information could be in feature measurement layer or in pose displacement layer. Our method calculates covariances as reliability measures in the both of these, which can be used as valuable information for fusion purposes. In a nutshell, intention of this work is to show that it is indeed possible to achieve real-time localization and mapping with a single laser range finder as the only data source. This is certainly of both theoretical and practical importance, particularly, when the only reliable data is the LRF's data.

2. RELATED WORK

Various sensors have been utilized to carry out the SLAM problem. However, the most impressive results in terms of mapping accuracy and scale have been reported for robots using laser range finder sensors. Main body of literature, relate on laser range scan matching, falls into two categories: point to point and feature to feature matching methods. The most popular point-wise methods usually follow the iterative closest point (ICP) algorithm. There are two fundamental simplifying assumptions in the ICP method, which are somehow optimistic and decrease this method's accuracy, as follows: *i) Matching assumption:* the corresponding points of two scans are successfully matched. *ii) Correspondence* assumption*:* the points of two scans, which are correctly matched with each other, correspond to exactly the same point of the environment's boundary.

Variants of ICP, such as [1], [2], [3], and [4], try to exclude ICP from these assumptions. However, consequent inaccuracy due to these assumptions is not completely eliminated. Besides, in these algorithms, computational complexity is in order of $O(n^k)$ in which $k>1$ and n is the number of scan points. In the point-wise approaches, n is approximately two orders of magnitude more than that in feature-based methods. Besides, because of the lack of features, the map, constructed using these algorithms, cannot be used for recognizing previously seen areas, and thus it would lead inevitably to drift in localization.

On the other hand, [5], [6], [7], and [8] are the state-of-art methods, which exploit natural features, extracted from range scans, for localization. Inability to closing loops, drift in localization, and lack of any reliability measure such as covariance for calculated pose shift are main drawbacks of these methods. Nevertheless, owing to the feature-based essence of these methods, they are more suitable for real-time applications. Besides, matching assumption here is more realistic in comparison with point-based methods, especially, if method exploit the local properties of scan around features

[9]. In addition, feature-based essence of these methods allows enriching the landmark-templates with the information collected from different sensors, such as cameras [10]. The addition of more information allows the building of high dimensional landmarks, which makes them more distinctive and makes the association process very robust [10].

3. FEATURE EXTRACTION

A concept that can be used to obtain salient features from the laser scan data is the local curvature value. Features extracted from local curvature are viewpoint invariant measures and, this means that they can be used as robust features in SLAM. In our system, features fall into two types: 1) Jump-edges which are scan measurements associated to discontinuities in scanning process. 2) High curvature points within segments, such as corners. Feature detection is composed of three main procedures: scan data segmentation, detection of high curvature points, and discarding variant features. There exist two cases in which variation is observed in features: i) The edges, which are established due to the occlusion, not to the real landmark in the environment. ii) When an edge of a segment established due to the sensors low range or lack of reflected laser beam, occurs when incidence angle between laser ray and obstacle's surface is about 0 or 180 degrees. Discarding these features made features' set reliable for SLAM. Figure 1 shows the extracted features and discarded ones from a sample scanned data.

In order to include these features in an EKF-based SLAM algorithm, it is necessary to estimate their uncertainties. Uncertainty of each feature has two major causes, rooted in physical properties of LRF: measurement process noise and quantized nature of rays' angles. Thus, if f_k is the true position of the $k'th$ feature of map (in robot's coordinate) and p_i is the candidate point of the scan for being $k'th$ feature, we have:

$$f_k = p_i + e_{ob,i} + e_{q,i} \tag{1}$$

In which $e_{ob,i}$ denotes the imposed error due to observation uncertainty and $e_{q,i}$ is the quantization error. Expected value and covariance of f_k has been calculated in [5]. Figure 2 shows the associated uncertainty with each of features previously shown in fig. 1. Shown ellipsoids are illustrated by the scaling factor of 10, indicating the 95 percent confidence region of each feature's covariance.

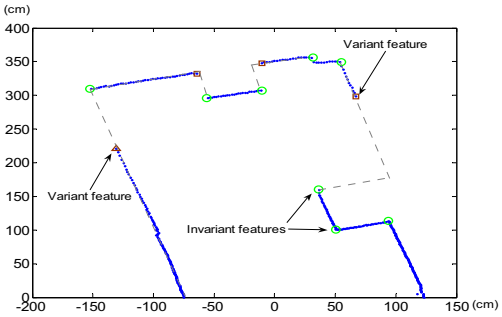

Fig. 1. Blue dots represent the scanned data, and dashed lines are ground truth of environment's boundary. Circles in green are extracted features of this scan. Squares are coinciding with variant features, which are established due to occlusion. Triangle shows a variant feature, which is established due to the lack of reflected ray. (Since incidence angle is near to zero.)

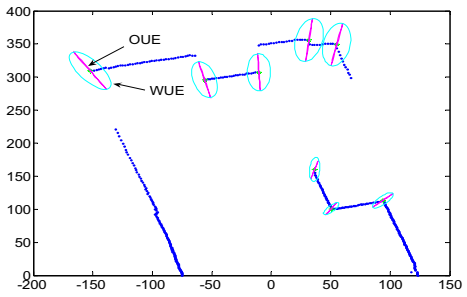

Fig.2. Extracted features from the scan, previously shown in fig. 1, along with their associated uncertainties. Ellipsoids in magenta represent the measurement covariance (OUE) of each feature and cyan ellipsoids (WUE) related to whole covariance of each feature, consisting of the observation and quantization errors.

4. MOTION PREDICTION

Every motion model, which is used in prediction stage, must stop at some level of detail and there exist some discrepancies between obtained model and reality. In traditional models for a wheeled robot, based on encoders' data, these discrepancies take account of factors such as wheel slippage, unequal wheel diameters, unequal encoder scale factors, inaccuracy about the effective size of wheel base, surface irregularities, and other predominant environmental effects which have not been modelled. These discrepancies are much more considerable in tracked mobile robots. Traditional prediction methods based on a model such as follows:

$$x_{k+1} = f(x_k, u_k, w_k) \tag{2}$$

One can consider the prediction procedure as a black box (see fig. 3a), whose outputs are expected value of the state prediction and covariance of this prediction. Here, alternative procedure is proposed for producing desired outputs, which is pictured in fig. 3b. This novel insight to prediction model comprises of three steps: matching step, an optimization process, which aims to predict robot's next pose, and uncertainty propagation step based on the implicit function theorem.

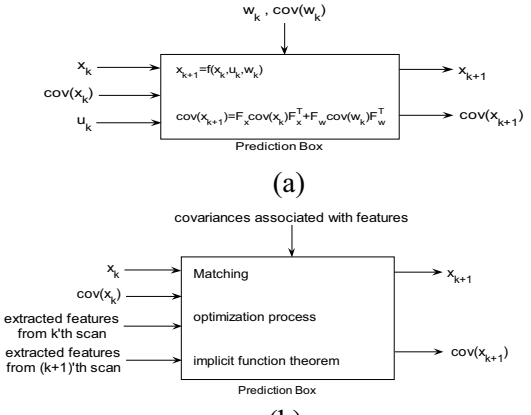

Fig. 3. a) Traditional prediction method, and b) Proposed prediction method.

Owing to the fact that features' topology cannot change fundamentally between two consecutive scans, adequate information is available for matching. Here, the matching method, proposed in [5], is adopted. In the second step, algorithm aims to predict robot's next pose through

calculating its displacement. Based on Gaussian-based maximum likelihood concept, following error function must be minimized (The hat symbol (^) above a variable, indicates its expected value.):

$$E = \sum_{j=1}^{m} (\hat{f}_{j,pre} - (R\hat{f}_{j,new} + T))^t C_j^{-1} (\hat{f}_{j,pre} - (R\hat{f}_{j,new} + T)) \quad (3)$$

m is the number of pairs resulted from matching algorithm. $F_j=[f_{j,new} \;\; f_{j,pre}]$ is *j'th* matched pair, and $f_{j,pre}$ and $f_{j,new}$ have been respectively extracted from the reference and new scans. $\nu_j = (\hat{f}_{j,pre} - (R\hat{f}_{j,new} + T))$ is the *j'th* innovation vector and C_j is its covariance. Assuming errors in two different scans are independent, one can write:

$$C_j = \text{cov}(e_{ob}^{pre} + e_q^{pre}) + R\,\text{cov}(e_{ob}^{new} + e_q^{new})R^t \quad (4)$$

Using quaternion, desired variables can be reshaped in vector form, $X=(q_1 \;\; q_2 \;\; t_1 \;\; t_2)^t$, in which

$$R = \begin{pmatrix} q_1^2 - q_2^2 & -2q_1q_2 \\ 2q_1q_2 & q_1^2 - q_2^2 \end{pmatrix} \;\; \& \;\; T = \begin{pmatrix} t_1 \\ t_2 \end{pmatrix} \quad (5)$$

t_1 and t_2 denote translations in x and y direction. To fulfil such optimization, linearization and iteration methods can be utilized [11]. Here, Sequential Quadratic Programming (SQP) method [12] is applied for solving this optimization problem. Owing to the fact that the number of summation terms in the objective function, equation 3, in feature-based methods is often reduced to 0.01 of that in point-based methods, SQP method produces an accurate solution for desired variables in a small portion of computing time.

Assume X^* is the robot displacement between two consecutive steps that minimizes E in equation 3; For calculating covariance of X^*, there should be a Jacobian that projects features' uncertainty onto X^* uncertainty. If there exists an explicit function, g, which relates X^* to F, vector of all matched features, then we have:

$$X^* = g(F) \;\; , \;\; F = [F_1 \;\; F_2 \;\; \cdots \;\; F_m] \quad (6)$$

Taylor expansion of g around *E[F]* results in:

$$X^* = g(\hat{F}) + (F - \hat{F})\frac{\partial X^*}{\partial F} + O(F - \hat{F})^2 \quad (7)$$

in which $O(.)^2$ denotes the terms of order 2 or higher. Jacobian between X^* and F projects uncertainty of F onto X^*.

$$\text{cov}(X^*) = J\,\text{cov}(F)J^T \quad (8)$$

However, there is no explicit function between F and X^*, and they relate to each other through an implicit function $I(X^*,F)=0$, which derived from $\partial E/\partial X=0$. The implicit function theory can provide such Jacobian via below equation:

$$J = -\left(\frac{\partial \Upsilon}{\partial X^*}\right)^{-1}\left(\frac{\partial \Upsilon}{\partial F}\right) \Rightarrow J = -\left(\frac{\partial^2 E}{\partial X^2}\right)^{-1}\left(\frac{\partial^2 E}{\partial F \partial X}\right) \;\; at \;\; X = X^* \quad (9)$$

Letting $E_j = v_j^t C_j^{-1} v_j$, yields to:

$$\frac{\partial^2 E}{\partial X^2} = \sum_{j=1}^{m} \frac{\partial^2 E_j}{\partial X^2} \quad (10)$$

(s,t) element of mentioned differentiation in equation 10 is calculated as follows:

$$\begin{aligned} \frac{\partial^2 E_j}{\partial X_t \partial X_s} = {} & 2\left(\frac{\partial^2 v_j}{\partial X_t \partial X_s}\right)^t C_j^{-1}(v_j) + 2\left(\frac{\partial v_j}{\partial X_s}\right)^t \left(\frac{\partial C_j^{-1}}{\partial X_t}\right) v_j \\ & + 2\left(\frac{\partial v_j}{\partial X_s}\right)^t C_j^{-1}\left(\frac{\partial v_j}{\partial X_t}\right) + \left(\frac{\partial v_j}{\partial X_t}\right)^t \left(\frac{\partial C_j^{-1}}{\partial X_s}\right) v_j \\ & + v_j^t \left(\frac{\partial^2 C_j^{-1}}{\partial X_t \partial X_s}\right) v_j + v_j^t \left(\frac{\partial C_j^{-1}}{\partial X_s}\right)\left(\frac{\partial v_j}{\partial X_t}\right) \end{aligned} \quad (11)$$

Calculations of current terms in equation 11 are complicated but a tractable matter of differentiation, which leads to a closed-form expression. For calculating second term in equation 9, firstly, it should be expanded:

$$\frac{\partial^2 E}{\partial F \partial X} = \left[\frac{\partial^2 E_1}{\partial F_1 \partial X} \;\; \frac{\partial^2 E_2}{\partial F_2 \partial X} \;\; \cdots \;\; \frac{\partial^2 E_m}{\partial F_m \partial X}\right] \quad (12)$$

(ix, jm)(s,t) element of $\partial^2 E/(\partial F_j\, \partial X)$ is calculated as follows:

$$\begin{aligned} \frac{\partial^2 E_j}{\partial (F_j)_t \partial X_s} = {} & 2\left(\frac{\partial^2 v_j}{(F_j)_t \partial X_s}\right)^t C_j^{-1}(v_j) + 2\left(\frac{\partial v_j}{\partial X_s}\right)^t C_j^{-1}\left(\frac{\partial v_j}{(F_j)_t}\right) \\ & + \left(\frac{\partial v_j}{(F_j)_t}\right)^t \left(\frac{\partial C_j^{-1}}{\partial X_s}\right)(v_j) + (v_j)^t \left(\frac{\partial C_j^{-1}}{\partial X_s}\right)\left(\frac{\partial v_j}{(F_j)_t}\right) \end{aligned} \quad (13)$$

Again calculating differentiations determined in equation 13, is tractable procedure. Substituting equations 11 and 13 into 9 yields to the desired Jacobian matrix. Independency of features in one scan leads to a block diagonal covariance matrix for their total covariance. Besides, assuming features, extracted from two consecutive scans, are independent, each pair's covariance takes the below form:

$$\text{cov}(F) = \begin{bmatrix} \text{cov}(F_1) & & 0 \\ & \ddots & \\ 0 & & \text{cov}(F_m) \end{bmatrix} \;\; , \;\; \text{cov}(F_j) = \begin{bmatrix} \text{cov}(f_{j,new}) & 0 \\ 0 & \text{cov}(f_{j,pre}) \end{bmatrix} \quad (14)$$

Now, substituting 9 and 14 into 8 results in the uncertainty of displacement. This covariance reveals the reliability of displacement estimation and can be used as valuable information for fusion purposes. Robot's pose at time step k is denoted by $x_{r,k}=[x_{r1,k}\; x_{r1,k}\; x_{r1,k}]$,in which $x_{r1,k}$ *and* $x_{r2,k}$ denote robot's position along x and y axis and $x_{r3,k}$ denotes robot's heading angle, all in step k. Robot's next pose is computed through below equation:

$$\hat{x}_{r,k+1} = \hat{x}_{r,k} + \begin{pmatrix} \cos\hat{\theta}_k & -\sin\hat{\theta}_k & 0 \\ \sin\hat{\theta}_k & \cos\hat{\theta}_k & 0 \\ 0 & 0 & 1 \end{pmatrix} \begin{pmatrix} t_1 \\ t_2 \\ \Delta\theta \end{pmatrix}, \; \hat{\theta}_k = \hat{x}_{r3,k} \quad (15)$$

In which t_1 and t_2 are translations along x and y axis, respectively, during time span between k and $k+1$. $\Delta\theta$ is the rotation angle during same interval and derived from $\Delta\theta = atan2(q_1, q_2)$. Calculating covariance of $X_{r,k+1}$, needs its differentiation with respect to stochastic parameters in the right-hand side of the equation 15.

$$J_p = \frac{\partial x_{r,k+1}}{\partial (x_{r,k}, q_1, q_2, t_1, t_2)} \quad (16)$$

Noticing to the dependency among the elements of the quaternion, J_p can be calculated as

$$J_p = \begin{pmatrix} 1 & 0 & -t_1\sin\theta_k - t_2\cos\theta_k & 0 & 0 & \cos\theta_k & -\sin\theta_k \\ 0 & 1 & t_1\cos\theta_k - t_2\sin\theta_k & 0 & 0 & \sin\theta_k & \cos\theta_k \\ 0 & 0 & 1 & -2q_2 & 2q_1 & 0 & 0 \end{pmatrix} \quad (17)$$

Regard to the independency of $x_{r,k}$ and X, Covariance of the right-hand side parameters of equation 15 takes the below form:

$$P' = \begin{pmatrix} \mathrm{cov}(p_k) & 0_{3\times4} \\ 0_{4\times3} & \mathrm{cov}(X^*) \end{pmatrix} \quad (18)$$

And thus the covariance of $x_{r,k+1}$ can be computed as

$$\mathrm{cov}(x_{r,k+1}) = J_p P' J_p^t \quad (19)$$

System's state vector, x_k, comprises of robot's state, $x_{r,k}$, and stacked state of all features, $x_{f,k}$. Now, let system's state vector and its covariance be as follows before prediction:

$$\hat{x}_k = \begin{pmatrix} \hat{x}_{r,k} \\ \hat{x}_{f,k} \end{pmatrix}, \mathrm{cov}(x_k) = \begin{pmatrix} \mathrm{cov}(x_{r,k}) & \mathrm{cov}(x_{r,k}, x_{f,k}) \\ \mathrm{cov}(x_{f,k}, x_{r,k}) & \mathrm{cov}(x_{f,k}) \end{pmatrix} \quad (20)$$

Robot's displacement does not affect features' state; therefore, outputs of prediction box take the bellow form:

$$\hat{x}_{k+1} = \begin{pmatrix} \hat{x}_{r,k+1} \\ \hat{x}_{f,k} \end{pmatrix},$$

$$\mathrm{cov}(x_{k+1}) = \begin{pmatrix} \mathrm{cov}(x_{r,k+1}) & \mathrm{cov}(x_{r,k}, x_{f,k}) J'^T_p \\ J'_p \mathrm{cov}(x_{f,k}, x_{r,k}) & \mathrm{cov}(x_{f,k}) \end{pmatrix} \quad (21)$$

Because of the fact that, uncertainty of robot's displacement is uncorrelated with the uncertainty of features in the map, J'_p is the truncated form of J_p includes only differentiation of $x_{r,k+1}$ with respect to $x_{r,k}$.

Finally, outputs of prediction box are listed as: $\hat{x}_{k+1}$ and $cov(x_{k+1})$, the predicted robot pose and associated covariance with this prediction, respectively. $\hat{x}^{(-)}_{k+1}$ and $\mathrm{cov}(x^{(-)}_{k+1})$ are the alternative notation for them, which will be used in filtering section.

5. FEATURE MEASUREMENT AND MAP UPDATE

For data association, firstly, the positions of the existing features in the map have to be predicted relative to the robot. This is accomplished through an observation model. Observation model for the *i'th* feature is as follows:

$$f_i^r = h_i(x_r, f_i^{map}) \quad (22)$$

In which $f_i = (f_{i1}, f_{i2})^T$ and Superscripts *r* and *map* denote the robot's and world's coordinates, respectively. Observation uncertainty has been calculated in [5] and distributed over features. In our system h_i takes the below form:

$$\begin{pmatrix} f_{i1}^r \\ f_{i2}^r \end{pmatrix} = \begin{pmatrix} \sqrt{(f_{i1}^{map} - x_{r1})^2 + (f_{i2}^{map} - x_{r2})^2} \\ \arctan(f_{i2}^{map} / f_{i1}^{map}) - \theta_r \end{pmatrix} \quad (23)$$

Total observation model, *h,* is obtained by considering all features in a single vector simultaneously as equation 6. Thus, it would be represented as a function of system's state vector, namely *h*.

Batch data association methods, where measurements are considered simultaneously, greatly reduce the ambiguity in data association process. Here, JCBB method [13] is adopted for data association. The features, which are not matched with any existent feature in the map, through data association process, are added to the map as new entries. On the other hand, features, which are matched with map's features, construct new relations between persistent objects in the map. In this case the system state vector and covariance matrix do not increase in size but constrained by the new relation and will be updated. Obtained information from sensors in current scan is described with a measurement function, equation 24.

$$\hat{F}^r = h(\hat{x}_r, \hat{F}^{map}) = h(\hat{x})$$
$$\mathrm{cov}(F^r) = H_x \,\mathrm{cov}(x) H_x \quad where \quad H_x = \left.\frac{\partial h(x)}{\partial x}\right|_{x=\hat{x}^{(-)}_{k+1}} \quad (24)$$

Because of the fact that process and observation models are not linear and in addition noise variables are assumed to be drawn from normal distributions, Iterated Extended Kalman Filter (IEKF) is chosen for filtering stage. The error in the estimation due to the nonlinearities in *h* can be greatly reduced by iteration, using IEKF. [14]

$$\hat{x}^{(+)}_{k+1,i+1} = \hat{x}^{(-)}_{k+1} + K_{k+1,i}[F^{k+1} - (h(\hat{x}^{(+)}_{k+1,i}) + H_x(\hat{x}^{(-)}_{k+1} - \hat{x}^{(+)}_{k+1,i}))]$$
$$\mathrm{cov}(x^{(+)}_{k+1,i+1}) = \mathrm{cov}(x^{(-)}_{k+1}) - K_{k+1,i} H_x \,\mathrm{cov}(x^{(-)}_{k+1})$$
$$K_{k+1,i} = \mathrm{cov}(x^{(-)}_{k+1}) H_x^T [H_x \,\mathrm{cov}(x^{(-)}_{k+1}) H_x^T + \mathrm{cov}(F^{k+1})]^{-1} \quad (25)$$

Where

$$H_x = \left.\frac{\partial h(x)}{\partial x}\right|_{\hat{x}^{(-)}_{k+1,i}}, \quad \hat{x}^{(+)}_{k+1,0} = \hat{x}^{(-)}_{k+1} \quad (26)$$

The *i'th* estimate of the state is used to evaluate the weight matrix, *K*, and is the argument to the non-linear sensor function, *h*. we observe that almost always after few, 2 or 3, iterations, there is little further improvement in the estimate and iterations can be terminated. The final estimate of the covariance need only be computed at the end of iteration, rather than at each step, since the intermediate system covariance estimates are not used.[1]

Fig. 4. Melon, the mobile robot equipped with low range laser scanners

[1] In EKF, process and observation models must be uncorrelated but in our work they seem to be correlated.

6. RESULTS

This section shows experimental results of the proposed method. Proposed method was implemented on the Melon, tracked mobile robot, which is equipped with two low range Hokuyo URG_X002 LRFs, span 360 degrees around robot (see figure 5.) The maximum measurable distance of these scanners are 4095mm. Their angular resolution per step is (180/512)=0.3515 degrees. Noise/maximum-range ratio in these laser scanners, are considerably more than high range sensors. In the experiments the following values are used by statistical analysis of measurement data: $\sigma_a=0.005$, $\sigma_b=1mm$ and $\sigma_\theta=0.001$ degree. All reported graphs are scaled in centimetres. Robot moves in a maze-type hand-made environment, similar to the one in Robocup rescue league.

First of all, we demonstrate pure localization results to verify accuracy and robustness of proposed process model. For the sake of comparison, we also reported the results of a point-wise and a feature-based method using the only LRFs' data (on the same data). ICP method [1] has been chosen as a popular point-wise method and HAYAI method [6] as the state of the art in feature-based methods. Figures 7a to 7c show the maps constructed by means of these methods. These maps are results of superimposing all scans gagged during drive in the environment. It should be mentioned that the only sensor used here is LRF and none of the map improving algorithms such as global relaxation [11] or cycle detection and correction [15] are considered in these experiments.

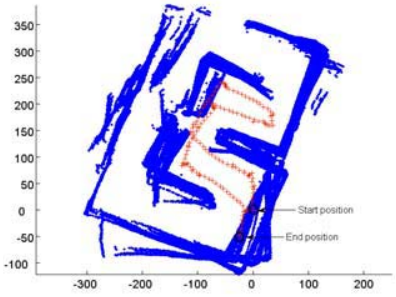

Fig. 7a. The map produced by ICP method using only LRF's data.

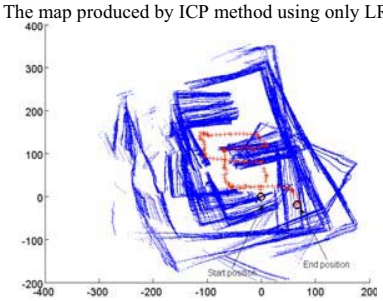

Fig. 7b. The map produced by HAYAI method using only LRF's data.

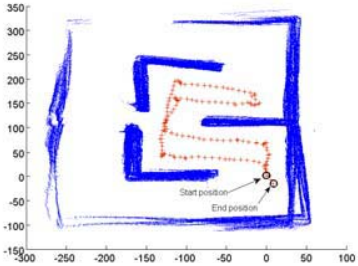

Fig. 7c. The map produced by proposed method using only LRF's data.

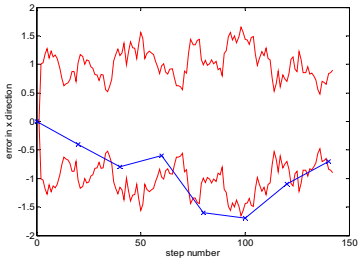

Fig. 8a. Robot's pose error in x direction, resulted in LSLAM. Maximum measured error is about 1.7 cm.

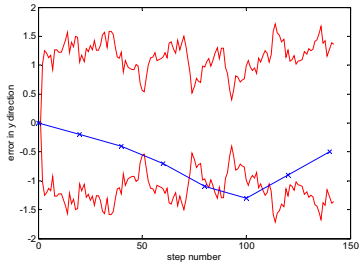

Fig. 8b. Robot's pose error in y direction, resulted in LSLAM. Maximum measured error is about 1.3 cm.

Figure 7a demonstrates the map, produced by the ICP method. Prior information about robot's displacement plays an important role in ICP-based methods, so that in the lack of such information, matching assumption is generally not satisfied. Also, ICP method suffers from correspondence assumption. These assumptions are the sources of ICP method's misreckoning.

HAYAI method produces impressive results in term of process speed [6]. However, in low range sensors with high noise and meager chance of capturing salient features, its accuracy declines (see figure 7b). The main reason of this imprecision rooted in feature extraction way of this method. It filters the scanned data at a fixed cut frequency so that it cannot extract features in different scales. Therefore, in the absence of highly salient features, it is inevitable to use filters with high cut frequency (which is the case in [6]). Nonetheless, such filters are not robust with respect to the noise and give rise to undesirable features. Besides, HAYAI does not reject variant features and also all features have the same contribution in pose shift calculation.

As it is shown in figure 7c, map is relatively well extracted by the proposed method. Exploiting iterative method for feature extracting, which uses different cut frequencies, method is capable to cope with noisy scanned data, to extract features of different scales, and to reject variant features. Calculating the reliability measure for features leads to a fair discrimination between their effects in robot's localizing based on their uncertainty. Finally, contrary to previous methods, owing to the both calculation of robot's displacement covariance and constructing an observation model, method has a potential to close loops and turn into full SLAM. To produce a ground truth of the trajectory, travelled during the experiment, robot stops at every 20 step and its accurate position is marked on the ground. Thus, comparison between estimated pose and ground truth is fulfilled in every 20 steps. Calculated errors in these steps are connected to each other via straight lines to construct a rough estimate of error curve along whole path.

Although maximum error and produced map (see fig. 7c) is acceptable for a pure localization method, in the presence of the noisy scanned data, converting the method from pure localization into SLAM restricts the errors in much less bounds. Standard deviation of error does not increase boundless and its limits are a function of number of features in the map, which come in the robot's field of view in varying sequences. Figure 8a proves this point visually. Due to the features distribution and the configuration of the path, travelled by the robot, most of the features in the environment remain in robot's field of view during significant interval of time. In other words, loops of many different sizes and interlinking patterns are frequently closed. Consequently, standard deviation of error does not intensify during robot movement. Fig 8b shows the same information about the robot's error in y direction.

Figure 9 shows the feature-based map at the end of path constructed by proposed SLAM method. Features and their associated covariances are shown in this figure. Solid lines depict the ground truth of the environment map. As it is seen in figure 9, features are well extracted and spurious features are rejected, and estimates of most of features are accurate. Zoomed view of the robot and a feature at the last step of the path are shown in figure 9b.

7. CONCLUSION

In this paper we have explained a method for SLAM, only based on the laser range finder data. The chief tents of our approach are *i)* introducing robust motion model with respect to robot slippage and inaccuracy in hardware-related measures, *ii)* calculating reliability measure for robot's displacement derived through the feature-based laser scan matching, *iii)* probabilistic mapping of extracted features, and *iv)* construct an IEKF framework merely based on laser range finder information. We have presented experimental implementations which demonstrate the applicability of the method, and we hope that it will have an impact in application areas in which other sensors data such as encoders' are not reliable. We have planned to generalize the method to 3D SLAM and also fuse the information, calculated in this method, with other sensors' information.

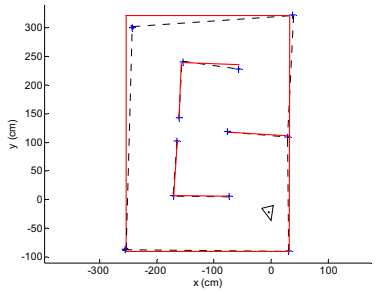

Fig. 9a. The feature-based map constructed by LSLAM.

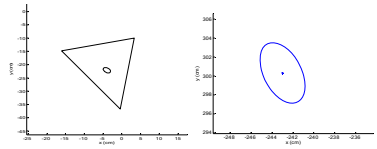

Fig. 9b. Left figure shows zoomed view of robot and the ellipsoid, which indicates the 95 percent confidence region of robot pose estimate by scaling factor 10, in the last step of path. Right figure demonstrates the zoomed view of a feature. The feature itself is shown by '+' and again associated ellipsoid represents its uncertainty.

REFRENCES

[1] *Robot pose estimation in unknown environments by matching 2D range scans.* **Lu, F. and Milios, E. 1997.** 1997, Journal of Intelligent and Robotic Systems, Vol. 18, pp. 249-275.

[2] *Metric-based scan matching algorithms for mobile robot displacement estimation.* **Minguez, J., Lamiraux, F. and Montesano, L. 2005.** Barcelona, Spain. : s.n., 2005. Proceedings of the IEEE International Conference on Robotics and Automation (ICRA).

[3] *Scan alignment with probabilistic distance metric.* **AJensen, B. and Siegwart, R. 2004.** 2004. Proceedings of the IEEE/RSJ International Conference on Intelligent Robots and Systems.

[4] *Weighted range sensor matching algorithms for mobile robot displacement estimation.* **Pfister, S., et al. 2002.** s.l. : Proceedings of the IEEE International Conference on Robotics and Automation (ICRA'02), 2002. pp. 1667-1674.

[5] *Feature-Based Laser Scan Matching For Accurate and High Speed Mobile Robot Localization.* **Aghamohammadi, A.A., et al. 2007.** s.l. : European Conference on Mobile Robots (ECMR'07), 2007.

[6] *High-speed laser localization for mobile robots.* **Lingemann, K., et al. 2005.** 4, s.l. : Journal of Robotics and Autonomous Systems, 2005, Vol. 51, pp. 275–296.

[7] *Natural landmark-based autonomous vehicle navigation.* **Madhavan, R. and Durrant-Whyte, H. F. 2004.** s.l. : Robotics and Autonomous Systems, 2004, Vol. 46, pp. 79-95.

[8] *Mobile robot positioning with natural landmark.* **Santiso, E., et al. 2003.** Coimbra, Portugal : s.n., 2003. Proceedings of the 11th IEEE International Conference on Advanced Robotics (ICAR'03). pp. 47-52.

[9] *Recursive Scan-Matching SLAM.* **Nieto, J., Bailey, T. and Nebot, E. 2007.** 1, s.l. : Journal of Robotics and Autonomous Systems, January 2007, Vol. 55, pp. 39-49.

[10] **Nieto, J. 2005.** Detailed environment representation for the slam problem. *Ph.D. Thesis.* s.l. : University of Sydney, Australian Centre for Field Robotics, 2005.

[11] *Globally consistent range scan alignment for environment mapping.* **Lu, F. and Milios, E. 1997.** : Autonomous Robots, 1997, Vol. 4, pp. 333–349.

[12] *An Interior, Trust Region Approach for Nonlinear.* **Coleman, T.F. and Y., Li. 1996.** s.l. : SIAM Journal on Optimization, 1996, Vol. 6, pp. 418-445.

[13] *Data association in stochastic mapping using the joint compatibility test.* **Neira, J. and Tardos, J.D. 2001.** 6, s.l. : IEEE Transactions on Robotics and Automation, 2001, Vol. 17, pp. 890–897.

[14] **Gelb, A. 1984.** *Applied Optimal Estimation.* s.l. : M.I.T. Press, 1984.

[15] *A real-time algorithm for mobile robot mapping with applications to multi-robot and 3D mapping.* **Thrun, S., Bugard, W. and Fox, D. 2000.** s.l. : International Conference on Robotics and Automation, 2000. pp. 321–328.